Supporting Information

Glutathione depletion-mediated *in situ* transformation of Prussian blue nanocubes for enhanced tumor-specific imaging and photoimmunotherapy

Shunxin Tang,‡[a] Bo Zhou,‡[a, b] Wanying Sun,[a] Chengyuan Zhu,[a] Yue Tang,[a] Bang-Ping Jiang,[a] and Xing-Can Shen*[a]

[a] State Key Laboratory for Chemistry and Molecular Engineering of Medicinal Resources, School of Chemistry and Pharmaceutical Science, Guangxi Normal University, Guilin, 541004, P. R. China.

[b] Scientific Research Center, Guilin Medical University, Guilin, Guangxi, 541199, People's Republic of China.

‡ S. Tang. and B. Zhou. contributed equally to this research.

*Corresponding Authors Xing-Can Shen

Email: xcshen@ mailbox.gxnu.edu.cn

Experimental Section

Materials, cell lines and animal models. Potassium ferricyanide ($K_3[Fe(CN)_6]$), $FeCl_3 \cdot 6H_2O$, polyvinylpyrrolidone (PVP), reduced glutathione (GSH), N-methylmaleimide (NMM) and α-lipoic acid (LPA) were purchased from Sinopharm Chemical Reagent Co., Ltd. Tetraacetoxymethyl ester (calcein-AM), 3,8-diamino-5-[3-(diethylmethylammonio)propyl]-6-phenylphenanthridinium diiodide (PI) and 3-(4,5-dimethylthiazol-2-yl)-2,5-diphenyltetrazolium bromide (MTT) were obtained from Sigma-Aldrich (Boston, MA, USA). Trypsin, fetal bovine serum and 1640 were obtained from Sangon. All of the ELISA kits and 2′,7′-Dichlorofluorescein diacetate (DCFH-DA) were purchased from Beyotime Biotechnology. L929, 4T1 and HeLa cells were acquired from the Chinese Academy of Sciences Cell Bank. The cells were cultivated with RPMI-1640 or DMEM including 100 units mL^{-1} penicillin, 10% FBS and 100 μg mL^{-1} of streptomycin in a suitable environment. Dendritic cells (DCs) were obtained from the bone marrow of naïve Balb/c mice, then cultured in the cell-culture medium with Granulocyte macrophage-colony stimulating factor (GM-CSF) for future use. The mouse purchased from Hunan SJA Laboratory Animal Co.，Ltd and were fed with sterilized water in a controlled environment (21 °C, 12:12 h light/dark cycle).

Synthesis of BG NCs and PB NCs. The BG NCs was synthesized by a facile one-

step approach. Briefly, PVP (30mg) and $K_3[Fe(CN)_6]$ (0.1 mM, 50 mL) were mixed to obtain a clear solution. Then, the solution was slowly added to 50 mL, 0.1 mM $FeCl_3$ aqueous solution under magnetic stirring for 72 h. Finally, the obtained green sediment was centrifuged and washed by deionized water and dried in an oven for 6 h at 80 °C. As a control, PB NCs were also prepared, and the synthesis process was similar to that of BG NCs, except that $FeCl_3$ was replaced by $FeCl_2$.

Characterizations and measurements. The morphologies of the as-prepared BG NCs, PB NCs and t-PB NCs were characterized by transmission electron microscopy (JEM-2100F, JEOL, Japan). UV-Vis-NIR spectra were recorded on a UV2600 UV-Vis-NIR spectrophotometer (Shimadzu, Japan). FTIR spectra were collected on a Perkin-Elmer FTIR spectrometer (Perkin-Elmer, U.S.A.). dynamic light scattering was performed a Malvern Zetasizer Nano ZS (Malvern Instruments, Ltd., Worcestershire, UK). X-Ray diffraction patterns were acquired on a Rigaku D/Max-2550V (Japan). Raman spectra were measured on a Raman confocal microscope (Renishaw Company, UK) excited at 514 nm and X-ray photoelectron spectroscopy was performed on an ESCALAB 250Xi X-ray photoelectron spectrometer (Thermo).

Photothermal properties. Photothermal images of the t-PB NCs were obtained by infrared camera (MAG30, Magnity Electronics, China). As a control, deionized water

and BG NCs were also tested.

Photothermal conversion efficiency of t-PB NCs. The photothermal conversion efficiency (η) of the t-PB NCs was determined by recording the change of the temperature of BG NCs and t-PB NCs under 808 nm laser irradiation until the solution reached a steady-state temperature. The value of η was calculated according to equation (2):

$$\eta = \frac{hA(T_{Max} - T_{Surr}) - Q_{Dis}}{I(1 - 10^{-A808})} \qquad (2)$$

where h is the heat transfer coefficient, A is the surface area of the container, T_{Max} represents the maximum steady-state temperature, T_{Surr} is the ambient temperature of the environment, Q_{Dis} represents the heat dissipation from the light absorbed by the solvent and the quartz sample cell, I is the incident laser power, and A808 is the absorbance of the sample at 808 nm. The value of hA is derived from equation (3):

$$\tau_s = \frac{m_D c_D}{hA} \qquad (3)$$

where τ_s is the time constant for the heat transfer of the system, which was determined from m_D and c_D as the mass and heat capacity of the DI water used to disperse the t-PB NCs, respectively.

Thermogravimetric analysis. BG NCs (with or without PVP modification) and PVP were collected, and heated from room temperature to 800 ℃ at a rate of 10 ℃ min^{-1} under N_2 atmosphere.

Detection of ROS *in vitro*. The produced ROS were measured using DCFH and DPBF. In a typical test, BG NCs, and a stock solution of DCFH or DPBF were mixed with or without adding GSH (5 mM). Then, the mixed solution was irradiated by 808 nm laser for 5 min, and the fluorescence or UV-vis-NIR spectra of the obtained supernatants after centrifugation was measured immediately. As a comparison, PB NCs were also tested.

Detection of the GSH/GSSG ratio. The ratio of GSH to GSSG were detected by colorimetric microplate assay kits. Briefly, GSH (1 mM) was mixed with BG NCs or PB NCs (200 μg mL^{-1}) for 15 min under vibration. Then, according to the manufacturer's protocol, the supernatant was collected after centrifugation used for GSH and GSSG levels assays, and the ratio of GSH/GSSG was determined.

Cytotoxicity assays of t-PB NCs *in vitro*. The cytotoxicity of t-PB NCs was measured by MTT assay on HeLa, 4T1 and L929 cell. Three kinds of cells were cultured in 96-well plates at 37 °C under 5% CO_2 for 18 h. Then 1640 medium with

different concentrations of BG NCs was added (0, 100, 150, 200, 300, 400 μg mL^{-1}) for 18 h to be transformed into t-PB NCs. Thereafter, the implants were discarded, and the MTT reagent was added for another 6 h to test the *in vitro* cytotoxicity by microplate reader.

Intracellular ROS detection. Intracellular ROS was measured using DCFH-DA. 4T1 cells were cultivated in confocal dish under the suitable conditions for 18 h. After treatment with BG NCs (400 μg mL^{-1}) or PB NCs (400 μg mL^{-1}) for 8 h, DCFH-DA (10 μM L^{-1}) was added for 1 h in the dark environment . An hour later, cells were washed by PBS and exposed to 808 nm laser for 10 min (0.8 W cm^{-2}). After irradiation, fluorescence images were acquired using a laser fluorescence microscope. The fluorescence intensity was monitored by flow cytometry. ROS detection in DC is similar to that in 4T1 cells.

***In vitro* phototherapy effects of t-PB NCs.** The phototherapy effect of t-PB NCs was also measured by MTT assays on HeLa and 4T1 cell. The cell culture conditions were similar to the cytotoxicity test. Thereafter, the cells were irradiated with 808 nm laser for 5 min at 4 °C (denoted as PDT only) or 37 °C (denoted as PDT and PTT). After 18 h of incubation, the cell medium was replaced with 200 μL of culture medium. Then, the MTT reagent was added to each well for another 6 h to test the *in vitro*

cytotoxicity with microplate reader. The photocytotoxicity was expressed as the percentage of viable cells compared to those in the untreated control group. If it was necessary to modulate the intracellular GSH, the cells will treat with LPA for 18 h or NMM for 40 min. Then, the GSH concentration-dependent phototherapy effect was also evaluated using the same method.

Intracellular Raman spectral analysis. After incubation with BG NCs for different times, the single-cell samples of the DCs 4T1 and L929 cell were analyzed by Raman spectroscopy using a Renishaw Raman spectrometer that used a krypton ion laser at a wavelength of 514 nm with a laser power of 1 % for an exposure time of 30s.

Co-staining assay. the cells were stained with PI (2%) and calcein-AM (1.6%) for 5 min before and after irradiation. Then, fluorescence images were taken before and after illumination.

***In vitro* and *in vivo* PA imaging.** PA imaging was carried out on a multispectral optoacoustic tomography (MSOT) system (inVision 128, iThera Medical GmbH, Neuherberg, Germany). For *in vitro* redox-enhanced PA signals generated by BG NCs, the BG NCs were incubated with different concentrations of GSH (0.2−5 mM) and then embedded in tubes for *in vitro* PA imaging. To study the ability of synthesis t-PB NCs in tumor tissue, PA images and PA signals were obtained after injection of BG NCs

(100 μL, 1 mg mL^{-1}) into the tumor site and normal tissue at different time points (i.e., 0, 10, 30, 60, and 120min).

***In vivo* Raman spectral analysis.** The mice bearing 4T1 tumors (approximately 50 mm^3) were subjected to an intratumoral and intramuscular injection with BG NCs (80 μL, 400μg mL^{-1}). After 6 h, the tumors and muscle tissue of the mice were stripped and detected by Raman confocal microscopy under laser excitation of 514 nm.

***In vivo* tumor growth study.** To evaluate the effect of phototherapy or immunotherapy, the subcutaneous 4T1 tumor-bearing Balb/c nude mice or 4T1 tumor-bearing Balb/c mice were divided into five groups (5 mice per group): (i) t-PB NCs + laser, (ii) PB NCs + laser, (iii) t-PB NCs only, (iv) laser only, and (v) the blank group. After the mice were treated, the body weight and the tumor size of each group were measured to evaluate the phototherapy efficiency. The volume (V) was calculated as V = (tumor length) × (tumor width)2/2. The relative tumor volumes were calculated as V/V0 (where V0 is the tumor volume before the treatment). The relative tumor volumes were monitored for 14 consecutive days. Finally, tumors were harvested and collected for H&E staining.

Blood Circulation. The 4T1 tumor-bearing Balb/c mice were administered BG NCs via tail vein injection. At different time points, whole blood was collected through the

orbital sinus, and were digest use a solution of HNO_3 and H_2O_2 (HNO_3:H_2O_2 = 3:1). After carefully filtering through a 0.22 μm membrane, each sample was subjected to ICP-OES to measure the concentration of Fe. The pharmacokinetic parameters were calculated using a reported model.

Histological assessment. The biocompatibility of t-PB NCs was evaluated using H&E staining. Balb/c nude mice were sacrificed at 14 days, and the histological changes of the major organ including heart, liver, spleen, lung and kidney were analyzed under optical microscope.

***In vivo* biodistribution assessment.** 200 μL saline (blank) or a saline solution of BG NCs (1 mg mL^{-1}) was injected into 4T1 tumor-bearing Balb/c nude mice via intravenous administration. The major organs, such as lung, heart, spleen, kidneys, liver and tumor were removed at different time intervals (12 h, 1, 4, 7 and 14 d) after injection and washed with PBS. Then, all tissues were dissolved by nitric acid, and the Fe content was performed by ICP-OES.

CRT and HMGB1 expression assays. 4T1 cells (1×10^5) were cultivated in 6-well plate overnight, after different treatment and incubated for 18 h,, washed with PBS, and stained with an Alexa Fluor 647-conjugated anti CRT antibody or PE anti-HMGB1 Antibody for 20 min. Image results were obtained from two-photon confocal

microscopy.

Extracellular ATP and HMGB1 release assays. 4T1 cells (1×10^5) were cultivated in a 6-well plate and incubated overnight. After different treatment and incubated for 18 h, the supernatant was detected using ELISA kits, according to the manufacturer's instructions.

Cytokine detection. Blood samples were removed from mice after different treatments. TNF-α, IL-6, IFN-γ were analyzed by ELISA kits according to vendors′ instructions.

Detection of immune cells in distal tumors. To study the infiltration of immune cells, distant tumors were harvested at day 8 from mice in different groups and homogenized into single cell suspension following the well-established protocol. $CD8^+$ and $CD4^+$ T cells were defined as $CD3^+CD4^+CD8^-$ and $CD3^+CD4^+CD8^-$, respectively. After removal of red blood cells (RBCs) by the RBC lysis buffer, these cells were stained with anti-CD4-FITC, anti-CD8-PE, anti-CD3-APC (BD Biosciences) (gated on $CD3^+$ T cells) antibodies according to the manufacturer's protocols. Mature DCs were defined as $CD80^+$ and $CD86^+$, and the collected cells from distant tumors were stained with anti-CD86-PE and anti-CD80-FITC. Finally, samples were detected by flow cytometer.

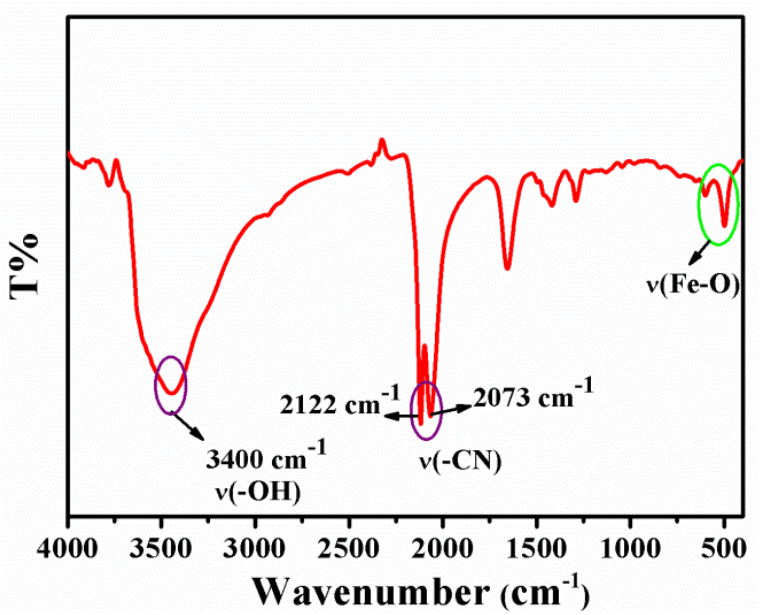

Figure S1. FTIR spectra of BG NCs.

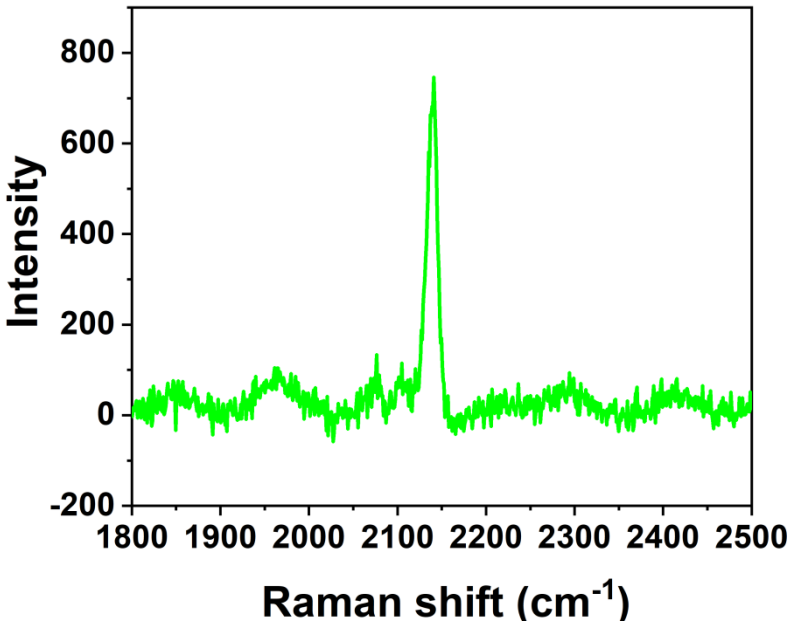

Figure S2. Raman spectra of the ν(CN) bands in BG NCs.

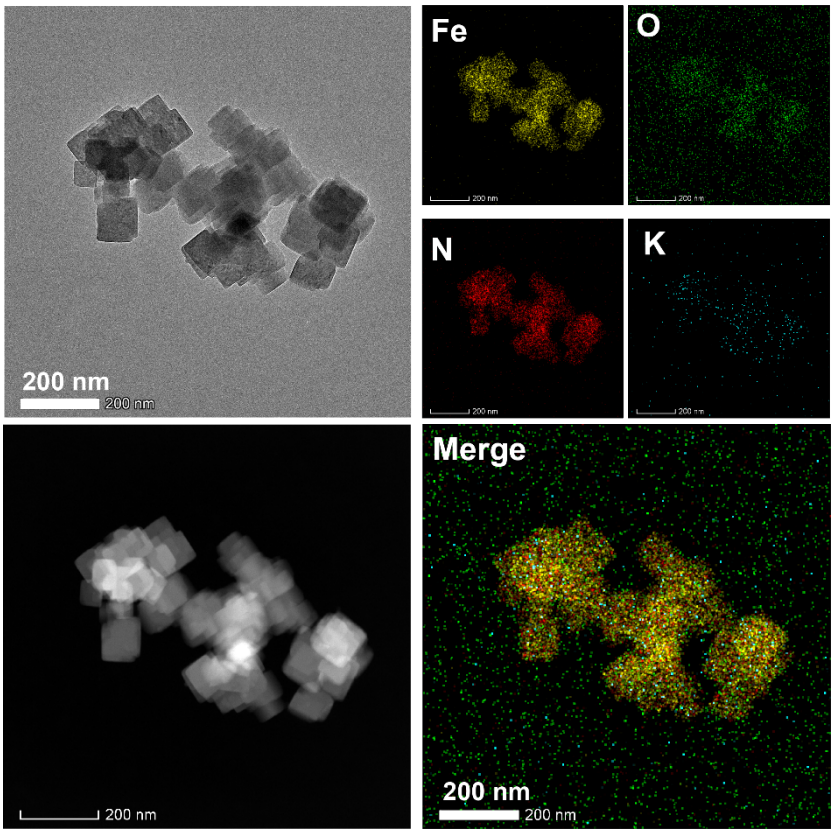

Figure S3. TEM and EDS elemental mapping spectrum of BG NCs. Scale bars 200μm.

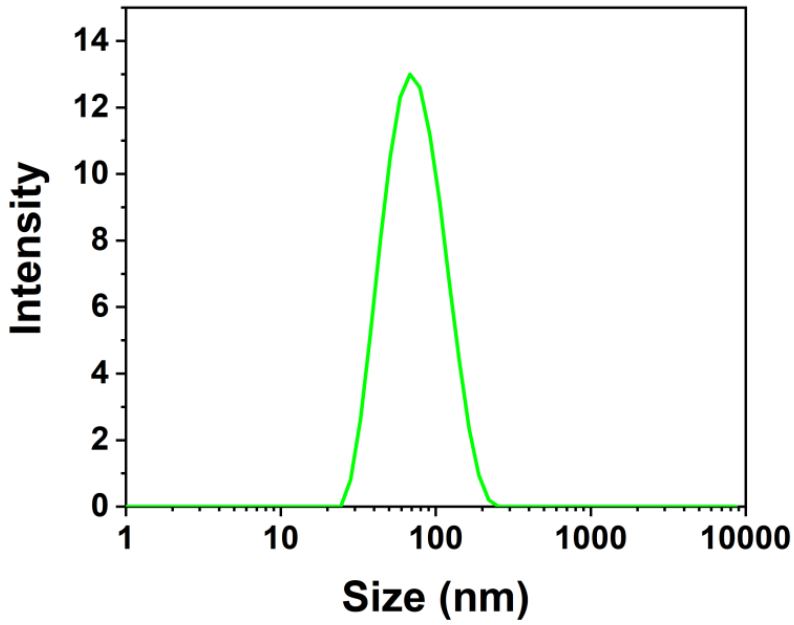

Figure S4. DLS of BG NCs in water.

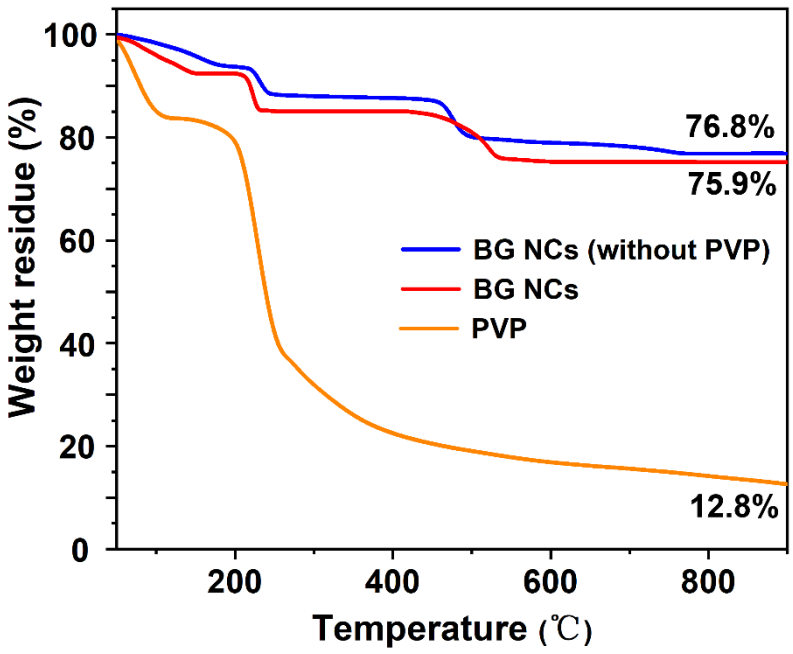

Figure S5. Thermogravimetric curves of BG NCs (with or without PVP modification) and PVP.

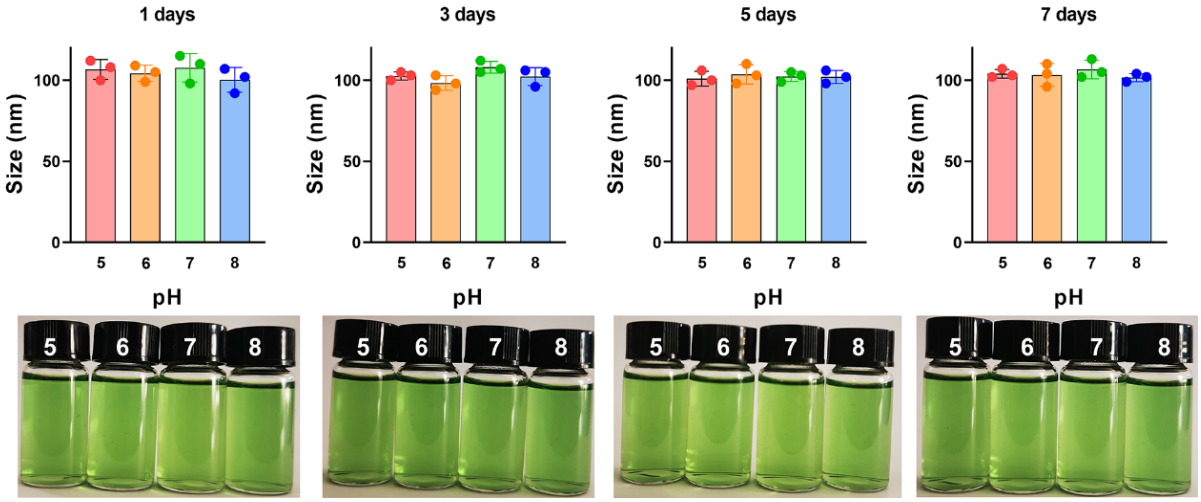

Figure S6. Time-dependent photographs and hydrodynamic size of BG NCs in water at different pH during the 7-day storage period, respectively.

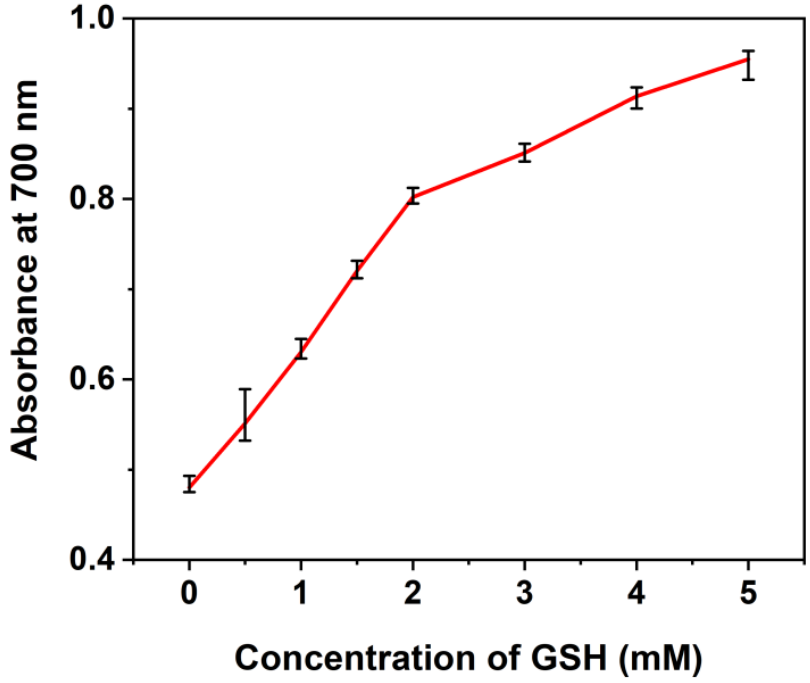

Figure S7. UV-vis-NIR absorption at ~700 nm of t-PB NCs after incubated with different concentrations of GSH.

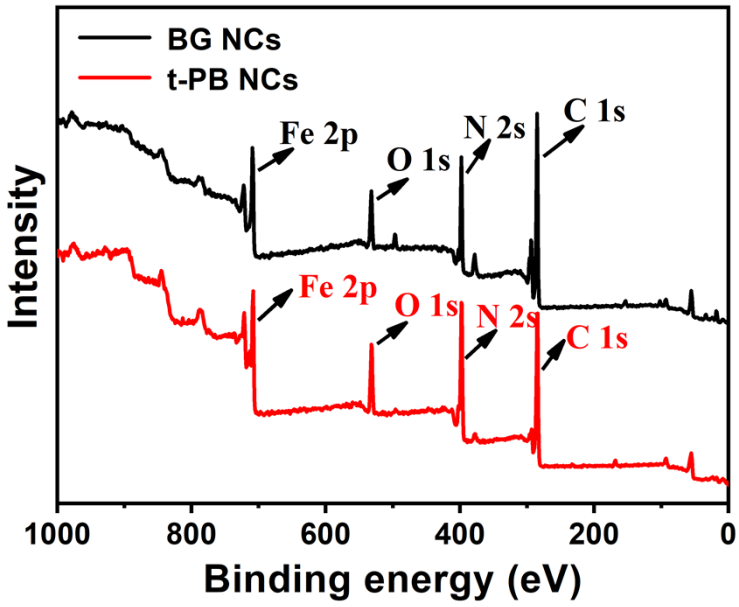

Figure S8. Full XPS spectra of BG NCs and t-PB NCs.

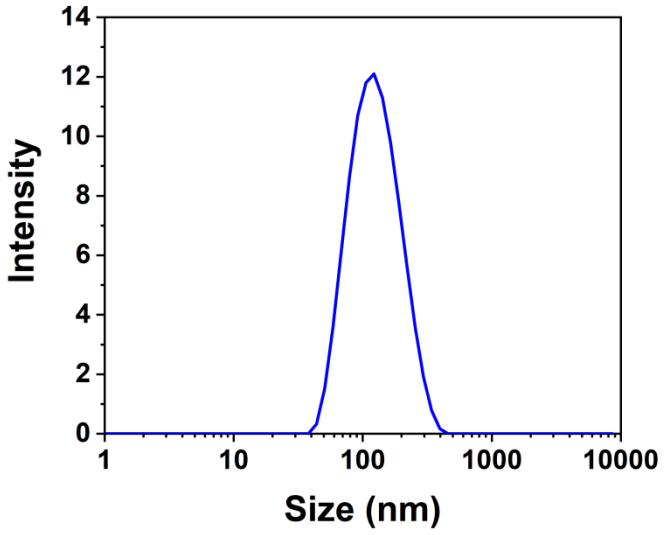

Figure S9. DLS of t-PB NCs in water.

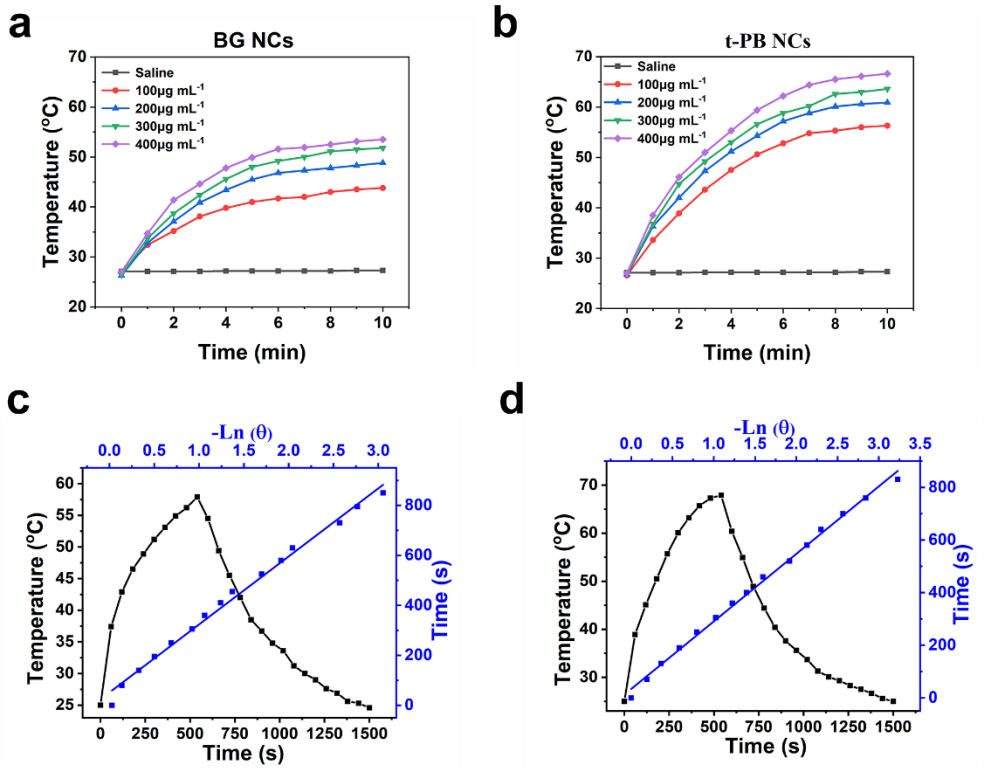

Figure S10. Photothermal heating curves of BG NCs (a) and t-PB NCs (b) in different concentration and the corresponding photothermal-conversion efficiency of BG NCs (c) and (d)t-PB NCs.

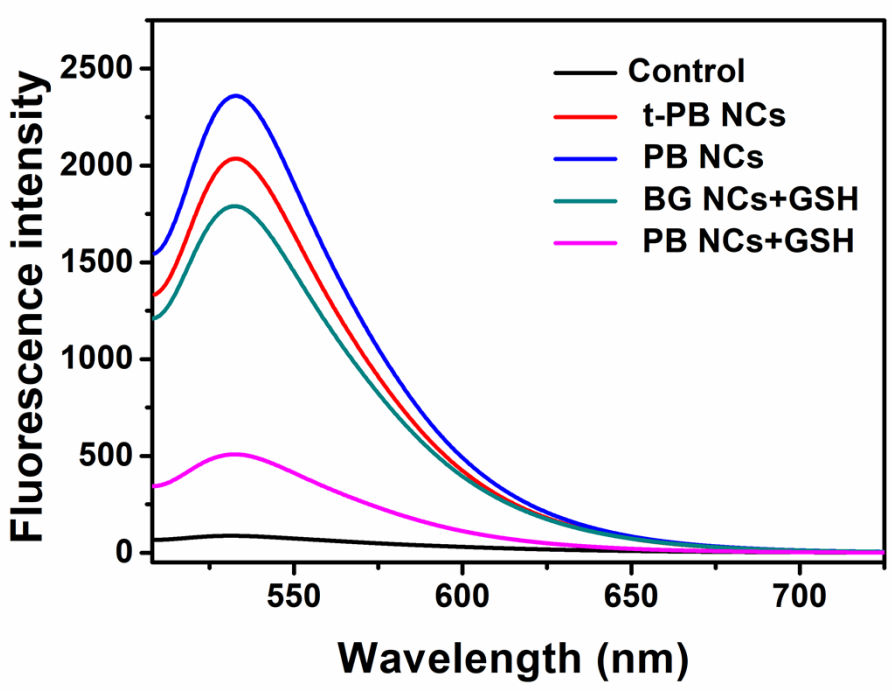

Figure S11. Fluorescence spectra of 2',7'-dichlorofluorescin (DCFH) cultured with PB NCs ort t-PB NCs in the presence or absence of GSH (5 mM) under laser irradiation.

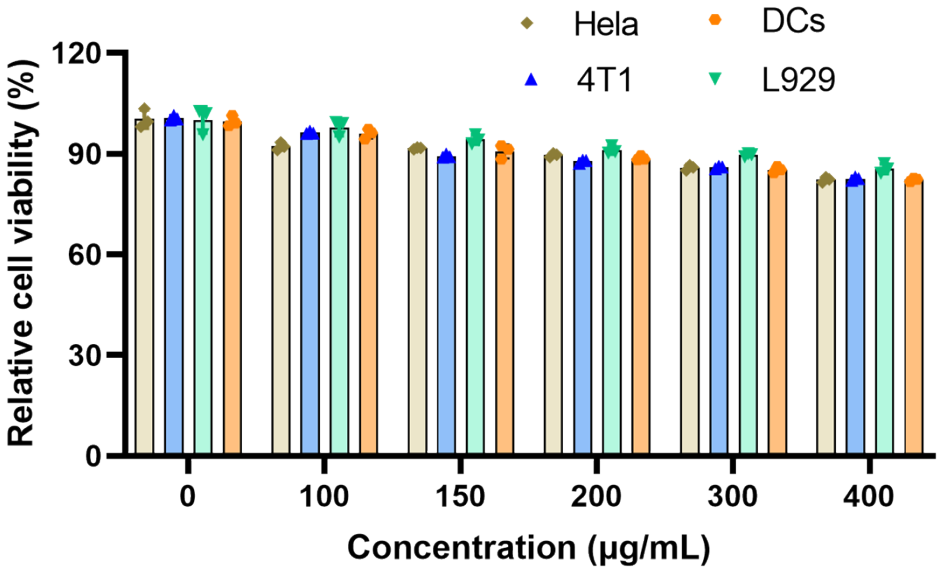

Figure S12. Dark toxicity analysis of the transformed t-PB NCs.

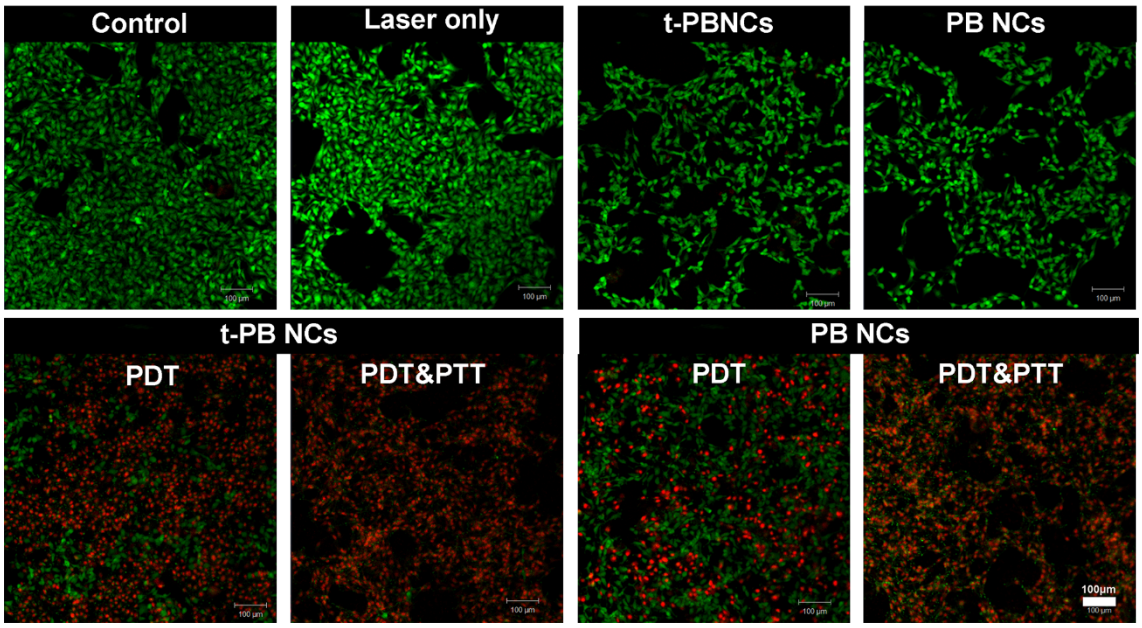

Figure S13. co-staining assay using PI (for dead cells, red fluorescence,) and calcein-AM (for live cells, green fluorescence) after different treatment. Scale bars, 100 μm.

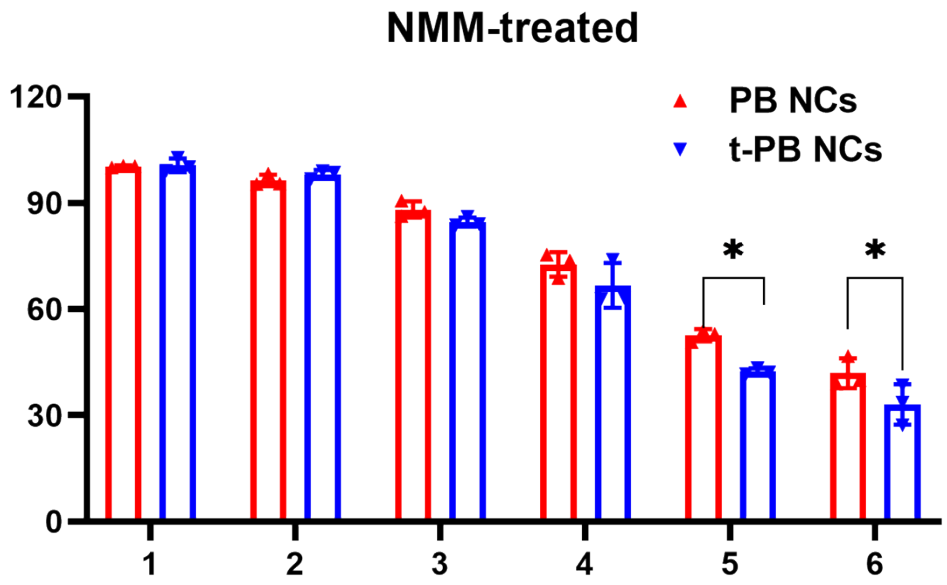

Figure S14. *In vitro* PDT effects of PB NCs and intracellular transformed t-PB NCs on NMM-treated 4T1 cells under irradiation.

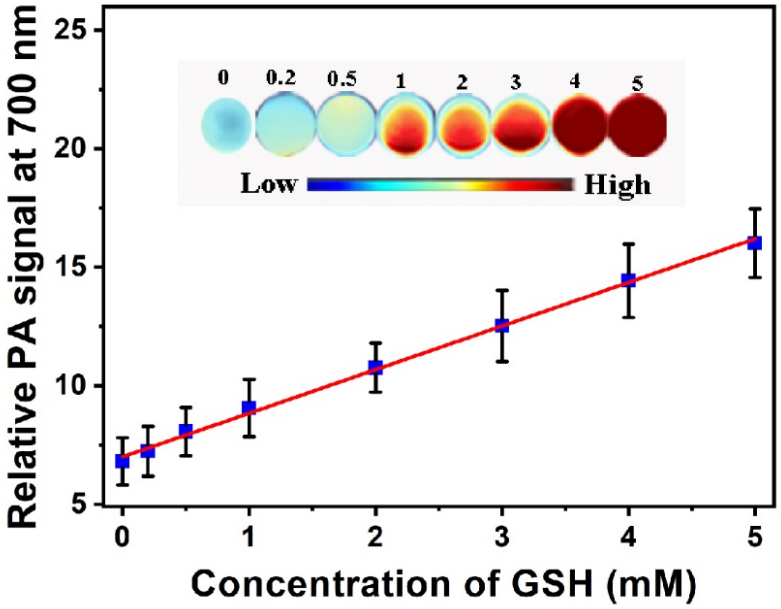

Figure S15. PA signal intensities of BG NCs after incubation with different concentrations of GSH. Inset PA images of the above solutions.

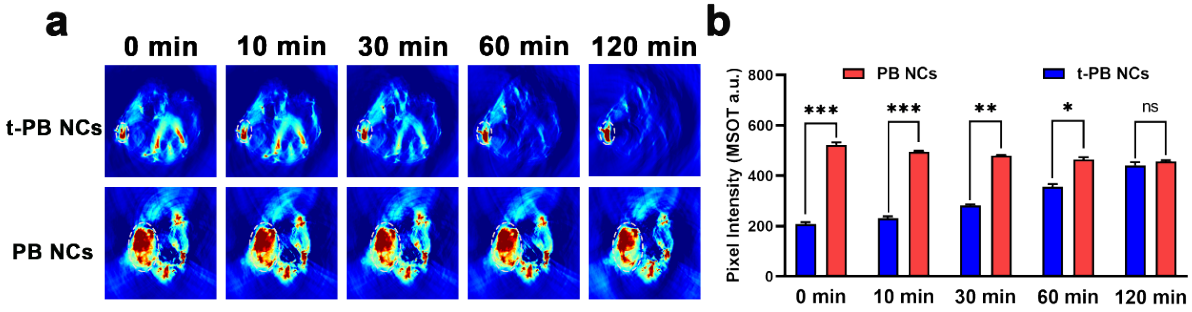

Figure S16. (a) *In vivo* PA images and (b) relative PA signal of 4T1 tumor-bearing nude mice post intratumoral injection of PB NCs or BG NCs.

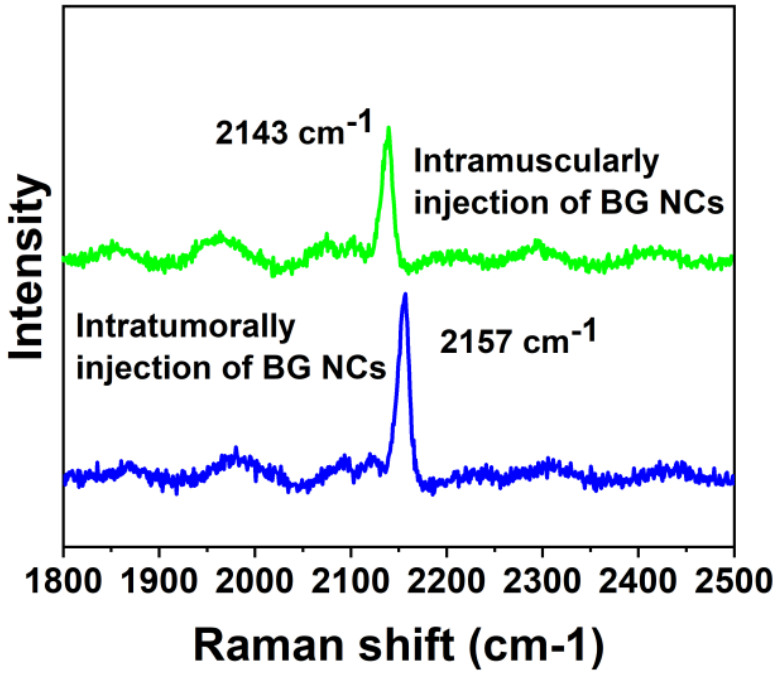

Figure S17. Raman spectra of the (CN) bands of t-PB NCs and BG NCs *in vivo*.

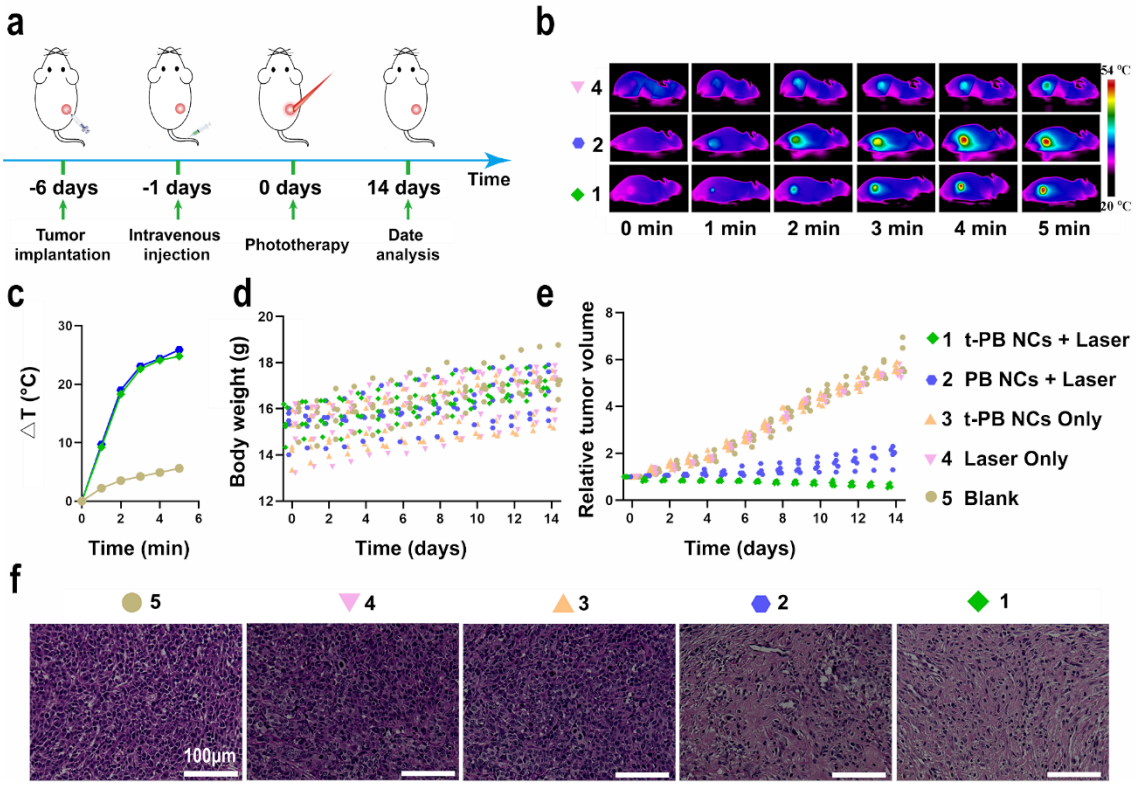

Figure S18. (a) Schematic illustration of the *in vivo* phototherapy enhancement experimental protocol. (b) IR thermal images and (c) corresponding temperature curves of 4T1 tumor-bearing mice after intravenous injection with saline, PB NCs and t-PB NCs under laser irradiation. (d) Tumor size trend of different groups after different treatments. (e) Relative body weight variation of the mice. (f) H&E staining images of tumors after different administration. Scale bars, 100 μm.

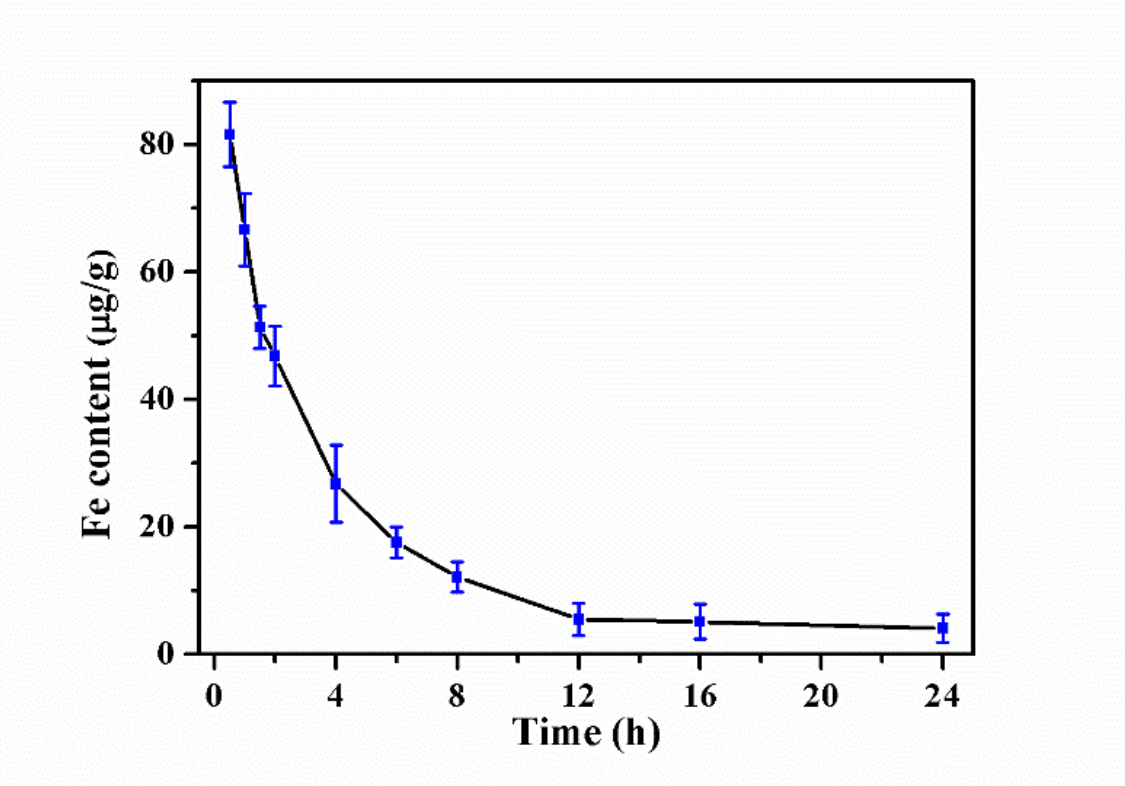

Figure S19. Time-dependent Fe content in the blood within 24 h after intravenous injection of BG NCs.

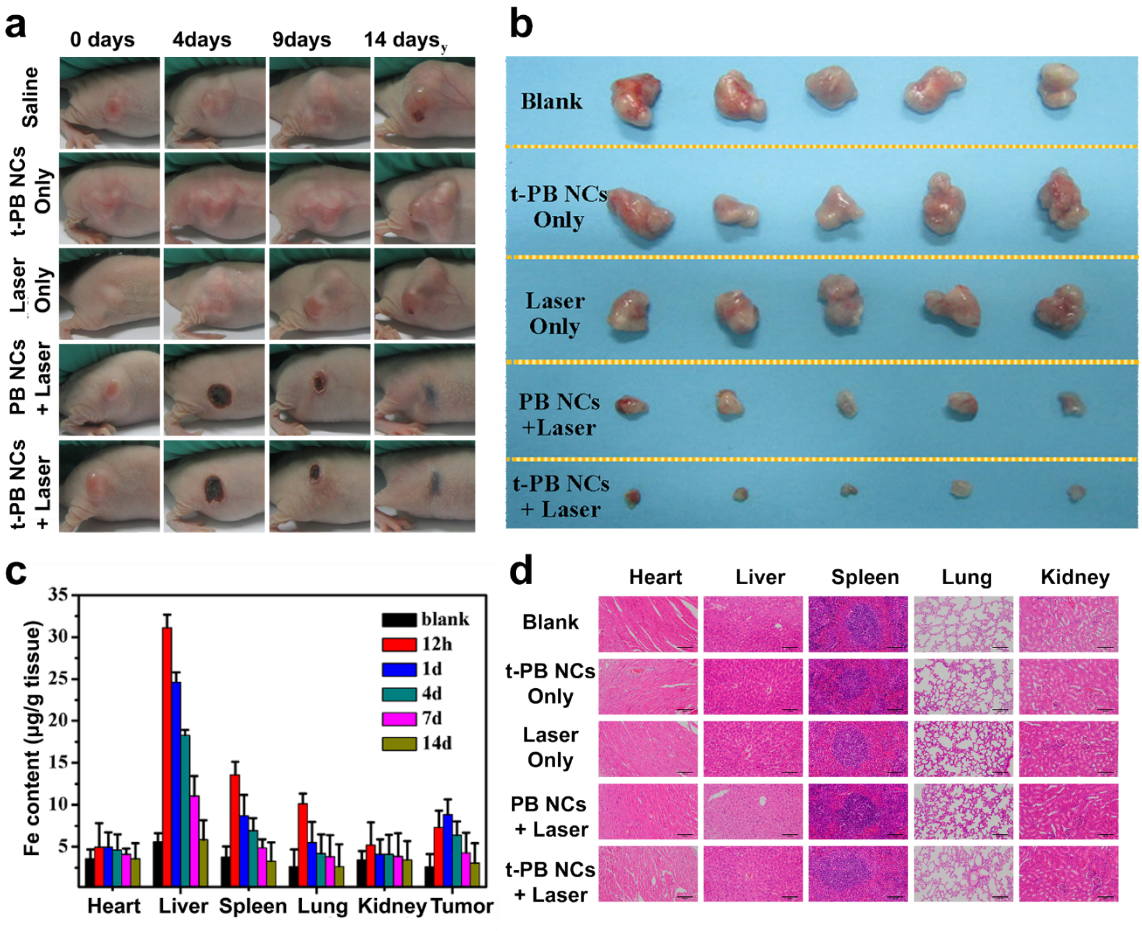

Figure S20. (a) Representative photos of Balb/c mice bearing 4T1 tumor before and after treatments for 0, 4, 9, 14 days. (b) Photographs of tumor tissues after various treatments. (c) Biodistribution of Fe in the main organs and tumor tissue after intravenous administration of saline (blank) and BG NCs (200 μL, 1 mg mL^{-1}) at different time points. (d) H&E-stained slices of main organs of on the 14th day after different treatments.

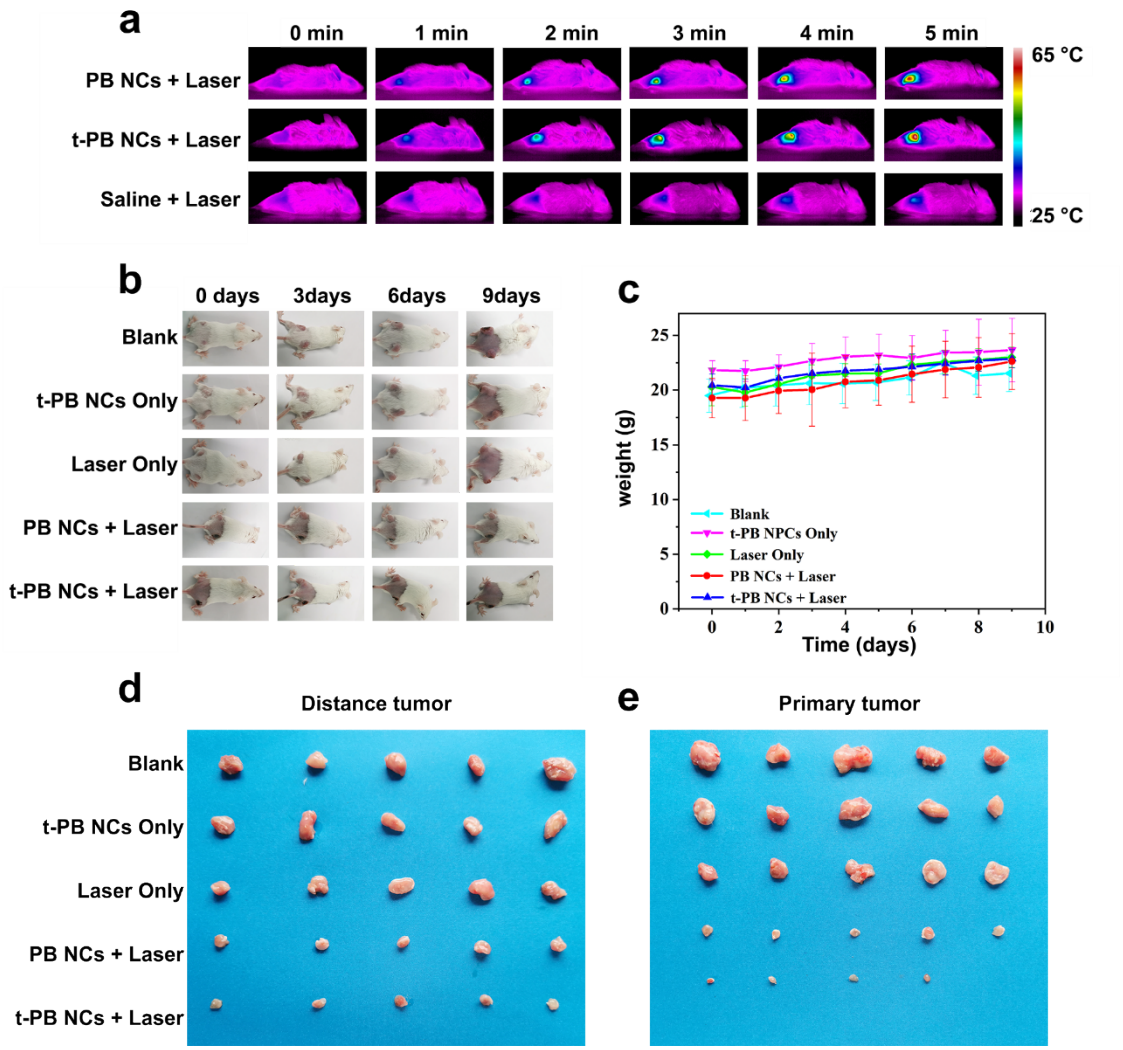

Figure S21. (a) IR thermal images of 4T1 tumor-bearing nude mice after intravenous injection with saline, PB NCs and t-PB NCs under laser irradiation. (b) Representative photos of mice bearing 4T1 tumor before and after treatments for 0, 3, 6, 9 days. (c) Relative body weight variation of the mice. (d) distance and (e) primary tumor size after different treatments.